International Journal of Current Engineering and Technology
E-ISSN 2277 – 4106, P-ISSN 2347 – 5161

Available at http://inpressco.com/category/ijcet

Research Article

Full-Scale Modeling of the Soil-Structure Interaction Problem Through the use of Hybrid Models (HYMOD)

George Markou†, Reem Sabouni†*, Farah Suleiman† and Rana El-Chouli†

†Civil Engineering Department, ALHOSN University, P.O.Box 38772, Abu Dhabi, UAE

Accepted 22 March 2015, Available online 29 March 2015, **Vol.5, No.2 (April 2015)**

Abstract

The research work presented in this paper deals with the modeling of the soil-structure interaction (SSI) by accounting for material nonlinearities while foreseeing the discretization of the superstructure through the use of hybrid-models (HYMOD) and the soil domain through the use of hexahedral elements that incorporate an elasto-plastic material model. In order to parametrically investigate this modeling concept, a full-scale 5-storey reinforced concrete building that was seismically strengthened was modeled and analyzed for different load combinations. Three models were considered in order to investigate the overall and local effects of the SSI phenomenon on the mechanical response of the structure for different loading scenarios, where the derived crack patterns and the building's foundation-soil interaction were investigated. The stress-strain development within the soil domain is also presented and discussed for both vertical linear static and horizontal nonlinear static loading conditions. The numerical investigation showed that the structure has met the seismic demands, and the raft slab which is used as the foundation system has helped minimizing any adverse effect of the SSI. Furthermore, the proposed modeling provided an in-depth analysis of the SSI problem in relation to the overall mechanical behavior of the RC structure. Finally, it was concluded that nonlinear modeling for ultimate limit-state loading conditions of SSI systems through the use HYMOD is computationally feasible; while the computational cost should be further reduced through the integration of ReConAn FEA with parallel solvers.

Keywords: *Soil-Structure Interaction, Pushover Analysis, Finite Element Analysis, Crack Propagation.*

Introduction

The inclusion of the soil structure interaction (SSI) in the seismic analysis of structures is considered beneficial in most seismic building codes, since it leads to higher damping of the system and lengthens the fundamental period of the structure. Post seismic observations of structures failing during recent earthquakes such as Bhuj (2001) and Sikkim (2011) earthquakes, illustrate the importance of the inclusion of SSI in the seismic design and they also demonstrate that the beneficial effect of SSI assumed in the code may be misleading, thus could lead to unsafe super and sub structural design (Ismail, 2014, Khoshnoudian and Behmanesh, 2010 and Mathew, *et al*., 2014). The most widely used analysis method to study the SSI is the time history analysis. The main advantage of this method is its ability to capture the structural response at any point of time during the analyzed earthquake. On the other hand, the uncertainty of the used ground motions, along with the complicity of performing the analysis, especially when detailed models are used, limits its use (Liu, *et al*, 2008). A widely used simplified approach to study the nonlinear dynamic response of structures is the pushover analysis. In the pushover analysis the studied structure is subjected to a monotonically increasing loading up to failure, and the nonlinear lateral force displacement relationships is recorded. This is used to estimate the structure's ultimate capacity and its seismic deformation demands (Panagiotidou, *et al*., 2012).

Due to the fact that a SSI investigation combines both fields of structures' and soil modeling; usually the detail level of such modeling is lower than that for the classical structural mechanics and soil mechanics standing alone. Most of the studies available in the literature on dynamic analysis of structures using pushover analysis and accounting for SSI, put more emphasis on the details of the super structure and tend to use simplified soil modes through mostly representing the soil by sets of springs. Several recent researchers such as Halkude *et al*. (2015), Mathew *et al* (2014), Baragani and Dyavanal (2014) and Ismail (2014) have studied the effect of accounting for SSI on reinforced concrete frames employing pushover analysis. The soil in these studies are modeled using

*Corresponding author: **Reem Sabouni**

the Winkler approach by equivalent linear springs with six degrees of freedom (three translational and three rotational). The frames are modeled with the standard beam element from the SAP2000 finite element analysis program. Some of the general conclusions that can be drawn from the previous studies, are that the fundamental natural period of the studied structures varied inversely with the stiffness of the soil, and that the lateral displacement decreased with the increase of the soil stiffness. Also it was found that as the base condition becomes more flexible the formation of the hinges increases.

Orakdogen *et al*. (2008) conducted a performance evaluation on a strengthened building considering SSI using pushover analysis. Several foundation options were evaluated (mat foundation, three different types of continuous footings and a single footing), while all of them were assumed to rest on tensionless elasto-plastic Winkler soil model. The elastio-plastic Winkler soil was modeled by equivalent frame elements subjected to axial forces only (no consideration for flexural or shear deformations was accounted for). The tension limit of the soil was taken as zero and the compression limit of the soil was calculated from the ultimate soil bearing capacity of the soil. The super structure was modeled as frame elements with the shear walls simulated as equivalent columns. This study concluded that the design and orientation of the building foundation system are very important for the seismic performance, and that the performance evaluation of a structure with a fixed-base condition may result in unexpected damage to the structure. Makhmalbaf *et al*. (2011) has conducted a pushover analysis study on short structures, accounting for SSI and also using the tensionless elastic plastic Winkler model. But the study utilized the gap element available in SAP2000 software to model the soil. The analysis of elasto-plastic SSI system using pushover analysis was also conducted by Liu *et al*. (2012). The horizontal and rocking constraints between the soil and foundation were modeled by horizontal spring-dashpot and rocking spring-dashpot systems respectively; whereas the frame's beams and columns were modeled using the beam elements. On the other hand, Panagiotidou *et al*. (2012) studied the pushover and seismic response of foundations on stiff clay with a more detailed 2D soil system. The soil was modeled (in ABAQUS software) using continuum solid plane strain four nodded bilinear elements and gap elements to simulate the foundation's potential uplift. The superstructure was modeled as a single lumped mass connected to the foundation by a rigid beam element.

In the current study a 3D detailed model is developed to discretize the soil-foundation system and foresees the discretization of both super and sub domains (half of the ground floor's columns and shear walls, the foundation and the soil domain) through solid finite elements. The HYMOD concept is used for the superstructure in order to decrease the computational demand of the numerical model, thus be able to perform the pushover analysis of a full-scale 5-storey RC building. The analyses are performed through the use of ReConAn FEA software where the developed models are analyzed in order to capture the full nonlinear structural response, with or without the SSI effect. The crack propagation developed in the foundation, ground floor columns and shear walls is also captured and studied through the implemented 3D detailed model, which is used within the HYMOD concept. The comparison between the models with and without SSI considerations is also presented.

1. Building Description and Materials

The studied building in this paper is a seismically strengthened 5-storey reinforced concrete (RC) building adopted from Orakdogen *et al*. (2008). As mentioned in the previous section Orakdogen *et al*. (2008) analyzed this building and studied the effect of SSI for different foundation types and loading conditions through the use of the Winkler model and SAP2000. This RC building is used herein so as to develop the numerical models that will be presented in section 2 of this paper.

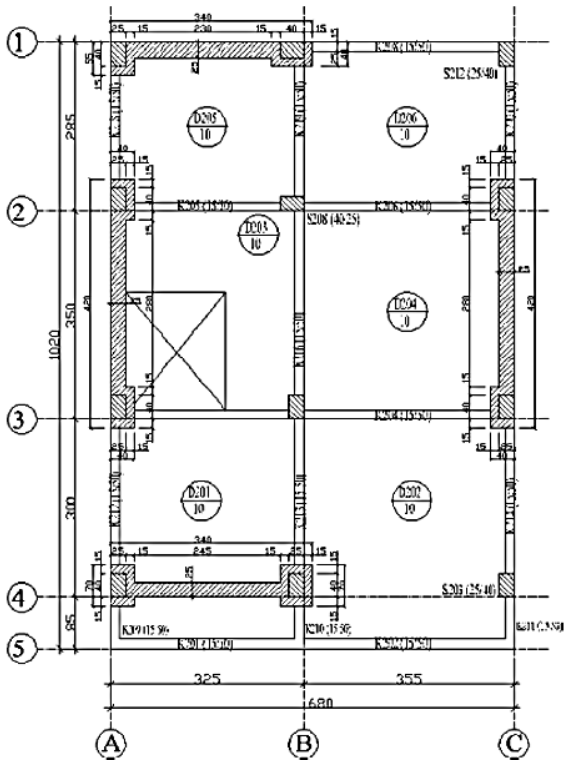

Figure 1 RC 5-storey building. Plan view. Orakdogen *et al*. (2008)

As it can be seen in Fig. 1, the initial framing system of the building consisted of 12 columns (with rectangular sections of 25x40cm) and drop-beams. The initial framing system was strengthened by constructing four main shear walls (3.4 and 3.5 meters long; two shear walls parallel to the x axis and two parallel to the y

axis) around the existing columns, as it can be seen in Fig. 1. The total length and width of the building's plan are 10.2m and 6.8m, respectively, while the total building height is 13.9m (the ground floor height is 2.15m, 3 typical floors have a 2.75m height each and the top floor has a height of 2.5m). The raft foundation's length, width and thickness are 8.80 m, 11.35 m and 0.70 m, respectively. The material properties of the structure are divided into two main groups: (a) existing RC material and (b) RC material used to strengthen the building. For group (a), the uniaxial compressive strength of concrete was reported to be equal to 16MPa and the steel reinforcement had a yielding stress of 220 MPa. For the case of group (b), the corresponding values were 20MPa and 420MPa, respectively. These were also the values incorporated in the numerical models presented in this paper.

2. Numerical Model

2.1 Modeling of the Superstructure

As it was presented by Markou and Papadrakakis (2014), modeling of RC structures can be performed by using different finite elements that derive various numerical responses, and their corresponding numerical accuracy depends on the adopted formulation. It is well known that beam-column elements can be used for the modeling of RC columns and beams, but their numerical accuracy when it comes to simulate the nonlinear behavior of shear walls is limited. For this reason the use of more accurate finite elements is required, like the 3D detailed modeling approach proposed by Markou and Papadrakakis, (2013), that provides a maximum numerical accuracy.

Their proposed modeling method (Markou and Papadrakakis, 2013) for 3D detailed modeling uses 8-node hexahedral isoparametric elements for the discretization of concrete where steel rebars are modeled through the use of embedded rod elements and may have any orientation inside the solid concrete elements, allowing the simulation of longitudinal as well as transverse reinforcement in a geometrically free manner. Concrete cracking is treated with the smeared crack approach as described in APPENDIX A. The material model used for concrete was the modified Kotsovos and Pavlovic material model (as proposed in Markou and Papadrakakis, 2013, see APPENDIX A) and for the steel rebars the Menegotto & Pinto model was used (see APPENDIX B).

When using the beam-column finite element for the superstructure modeling, the computational demand is minimized, but the finite element's formulation is unable to capture the mechanical behavior of shear dominated members like shear walls, especially for cases of ultimate limit state push over analysis (Markou and Papadrakakis, 2014). On the other hand, when more accurate models are involved (i.e. 3D detailed models) the corresponding computational demand increases significantly while it can lead to models that require days or even weeks to be solved. In an attempt to overcome this modeling issue, Markou and Papadrakakis, (2014) proposed the hybrid modeling approach HYMOD, where the shear dominated structural members are discretized through the use of the 3D detailed model (Markou and Papadrakakis, 2013) while the rest of the structural members are modeled through the use of the natural beam-column flexibility-based finite element NBCFB (Markou 2011). The NBCFB element is also integrated with the fiber approach and the numerical ability of accounting for the behavior of concrete and steel materials through the use of the Kent & Park (see APENDIX C) and Menegotto & Pinto models, respectively (for more details see Markou 2011).

The HYMOD approach was implemented in this case so as to develop the full-scale RC frame of the building, as it is shown in Fig. 2, where the raft slab and half of the ground floor are modeled through the use of the 3D detailed modeling concept thus the rest of the structure is discretized through the use of NBCFB elements in order to decrease the computational demand of the final model. The slabs were modeled through the use of rigid beam elements for all developed models. The model described in this paragraph is called Model B throughout this paper.

One of the main challenges when modeling the SSI problem is the ability to develop a detailed 3D model for both the super structure and substructure together using the finite element method and still be able to have reasonable computational cost. The use of the proposed HYMOD will allow the capturing of the 3D geometry of the foundation including the 3D geometry of the soil domain along with a sufficiently detailed superstructure. When using the HYMOD approach the foundation and soil domains can be directly discretized through the use of 8-noded hexahedral elements thus the derived mesh is geometrically accurate without the need of implementing any simplification assumptions.

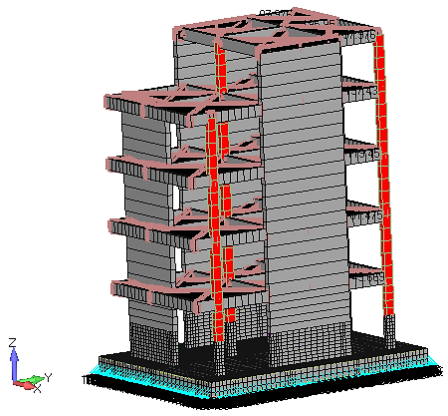

Figure 1 HYMOD finite element mesh of the 5-storey building. HYMOD model with fixed base (Model B).

In addition to the model illustrated in Fig. 2 which considers that all the nodes on the base of the raft slab are fixed, a model that uses only NBCFB elements was

constructed (Model A) so as to investigate the shear deformation effect and compare the derived results from the push over analyses with the numerical results derived from the HYMOD model. As it is going to be presented in the next section, an additional model was also constructed that uses the mesh shown in Fig. 2 in order to discretize the foundation and superstructure, while the fixed support assumption was substituted by the soil domain that was discretized through solid elements in order to account for the SSI effect. This model is called Model C throughout this paper.

2.2 Modeling of the Foundation and Soil Domains

As it is shown in Fig. 3, the raft slab that was considered herein as the system used to transfer the superstructure loads to the soil domain, was discretized through the use of the 8-noded hexahedral element. The 12 mm in diameter reinforcement cage was discretized through the use of the embedded rod element (see Fig. 3).

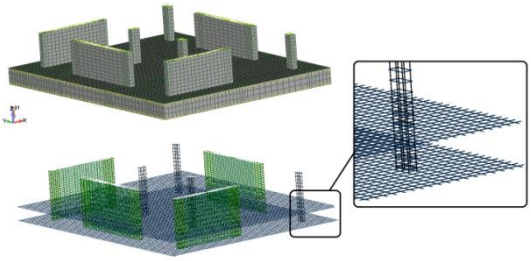

Figure 2 Hexahedral and embedded rebar mesh of the raft foundation and the ground floor's columns and shear walls.

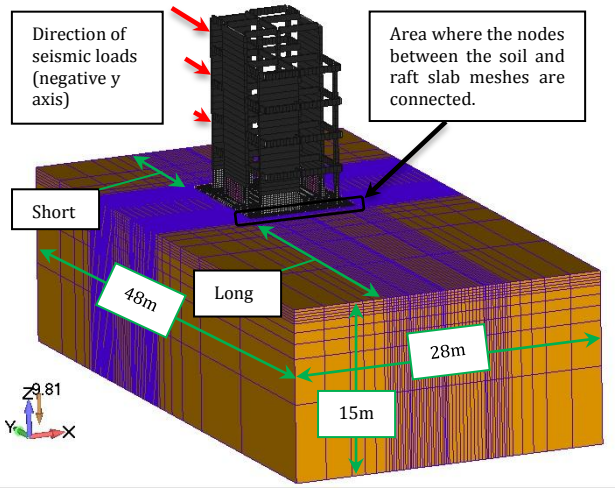

Figure 3 HYMOD model with soil mesh (Model C). Model developed for push over analysis.

The 3D mesh of the foundation system was directly connected to the finite element mesh that was developed to simulate the mechanical response of the soil domain which also foresaw the use of the 8-noded hexahedral element. Fig. 4 illustrates the final finite element mesh of the model that was used to perform the push over analysis and considered the SSI phenomenon. A total of 68,985 elements were used to discretize both the superstructure and the soil domains. This model was also modified (remove the soil elements that surround the raft slab) so as to apply the dead loads only (Model D).

2.3 Mesh considerations and boundary assumptions

When modeling the soil domain in 3D under SSI conditions the dimensions of the soil mesh play a significant role on the overall accuracy of the final model. This is always the case when dealing with SSI dynamic analysis where the wave propagation combined with numerical effects related to the boundary conditions implemented on the soil mesh's nodes, can alter the numerical results and eventually modify the numerical response of the numerical model. This also applies for 2D models as described by Panagiotidou *et al*. (2012) thus special boundary conditions should be implemented. For these reasons, when dynamic analysis is considered, the dimensions of the soil domain should be at least 4 times the corresponding raft slab foundation width (Zhao and Wang, 2008).

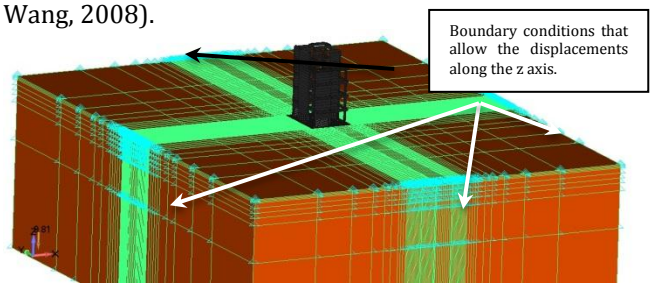

Figure 4 HYMOD model with initial soil mesh.

An initial model was developed as presented in Fig. 5 that incorporated this recommendation, and it was found to be computationally demanding. The model in Fig. 5 required almost a day so as to complete the calculations of a single load increment therefore it could not be used to perform a full push over analysis. For this reason a parametric investigation related to the optimum soil mesh size was performed, while the numerical effect on the results of the overall soil mesh size was investigated. As it resulted through this parametric investigation, the derived settlement for different models that assumed reduced soil mesh dimensions was found to be the same. When only the self-weight of the structure was considered (including dead loads), the settlement did not change for different x and y dimensional reductions of the soil mesh, thus it was concluded that the static nature of the load did not require a large soil mesh along the x and y axes (the height of the soil mesh along the z axis was considered to be constant and equal to 15m). In addition to that, the soil finite element size around the foundation was relatively fine for all considered models (hexahedral edge lengths vary between 10-30cm), therefore the overall numerical behavior that derived from all SSI

models managed to capture the mechanical response of the soil with the same numerical accuracy (stress-strain development under the foundation was in all cases the same; see section 3).

Fig. 6 shows the deformed shape and the von Mises contour as they resulted from the analysis when only the dead loads are applied. In order to avoid any shear stiffness development between the raft slab and the soil domain, the hexahedral mesh of the soil was not connected to the raft slab's nodes located at its perimeter (70cm interface with the soil material at the perimeter of the raft slab, see Fig. 6; Model D). It must be also noted at this point that the soil domain's boundary nodes (at the perimeter) were allowed to displace freely along the z axis while their x and y degrees of freedom were constrained (see Fig. 5). This way the soil mesh was free to settle at any point within the model but the nodes located at the base of the soil were fixed.

The soil's material properties that were used in the elasto-plastic von Mises material model that was used to simulate the nonlinear response of the soil, were equal to E_s = 1,601,600 kPa (Young modulus) and the ultimate stress was f_u = 900 kPa. The analysis of the vertical static loads resulted in a maximum foundation settlement equal to 1.33 mm, which was mainly attributed to the soil's deformation due to the superstructure loads.

An additional reduction of the soil mesh was performed based on the direction of the applied seismic loads (y-axis), as it can be also observed in Fig. 4 (short and long dimensions of the soil mesh that is located behind and in front of the foundation, respectively). The dimension parallel to the x-axis of the soil mesh is smaller than the y-dimension given that this model was developed to analyze the case where the seismic loads are applied along the negative y axis. Because the structure is pushed by a static horizontal load parallel to the y-axis, the soil elements located on the left and right far distance from the foundation are going to develop minor deformations due to the SSI thus are reduced. Furthermore, the overturning moment due to the seismic load (Model C) caused a non-uniform stresses distribution under the foundation with a larger stress towards the front of the foundation and a smaller stress towards the back of the foundation. The stresses at the foundation back edge were close to zero but no uplift occurred (no gaping between soil and foundation). Due to this stress distribution the soil at the fare region behind the foundation had marginal effect on the analysis results, thus the size of the soil behind the foundation was reduced (short in Fig. 4) to decrease the computational time required for the analysis. The final soil mesh dimensions that were adopted and used during the push over analysis were 28x48x15m (x, y and z axes, respectively).

Another significant modeling issue that immerses when 3D solid modeling is used to discretize both domains (RC foundation and soil) is the interface behavior and its numerical response when under tension due to possible uplifts. ReCoAn FEA has the ability to use the smeared crack approach thus use hexahedral elements with zero tensile strength. These elements can be used as interface elements to decouple the RC raft slab from the soil domain in case of partial foundation uplifts. When these elements are under tension they develop cracks thus lose their tensile stiffness and ability to transfer any stresses to the soil mesh. Nevertheless, this approach was not required herein, given that the push over analysis revealed that the raft slab did not develop any uplifts.

Before moving to the next section, it must be noted that the raft slab's nodes located on the perimeter of the foundation that is expected to develop compressive stresses due to the interaction with the soil (raft slab will push the soil within that region due to the horizontal applied forces) are connected to the soil's nodes (see Fig. 4, Model C). The other three sides of the raft slab's perimeter are not connected to the soil mesh similar to what it was implemented and presented in Fig. 6 (Model D has all sides disconnected from the soil mesh in order to avoid the development of shear resistance between the raft slab's sides and the soil domain).

3. Results and Discussion

The main objective of this research work is to perform a preliminary SSI analysis by using the 5-storey RC building presented in the previous section, thus examine the feasibility of performing this type of full scale simulations by considering a 3D approach while investigate the SSI effect of the at hand model when push over analyses were considered. The seismic assessment of the building is also within the same scope and in accordance with seismic demands reported by Orakdogen *et al.*, 2008 (the seismic demand was reported to be less than 1000 kN for all foundation types). For this reasons a total of three models were developed and analyzed for both dead and seismic load scenarios. These three models were as follows:

A. Model A: Model with NBCFB elements only and fixed base.
B. Model B: HYMOD model with fixed base (Fig. 2).
C. Model C: HYMOD model with soil developed for the push-over analysis (Fig. 4).
D. Model D: HYMOD model with soil for applying only the dead loads (Fig. 6).

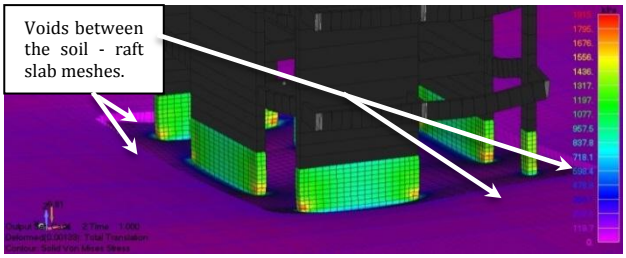

Figure 5 Deformed Shape and von Mises stress contour (kPa) – model with soil mesh developed for applying the dead loads only (Model D).

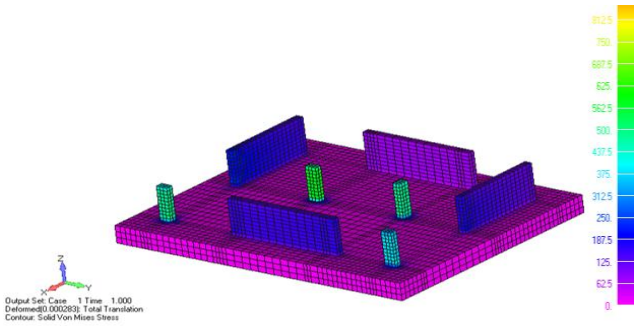

Figure 6 Deformed Shape and von Mises stress contour (kPa) due to the dead loads – model B.

As it was stated in section 2, the dead loads were applied on a modified model C (Fig. 6) where the stress contour indicates a maximum von Mises stress at the shear walls due to the deformation of the raft slab that derives from the SSI effect. Even though the raft slab (70cm thick) is behaving in a rather stiff manner, the stress development at the columns and shear walls was not found to be the same with the stress development that resulted from model B (HYMOD model with fixed base).

Due to the raft slab's deformation (that was attributed to the SSI) the stresses within the ground floor structural members were found to be increased (with a maximum von Mises stress of 1950kPa) especially at the shear wall section's ends (see Fig. 6). When the dead loads were applied on Model B the raft slab remained practically undefromed given that all the base nodes were considered to be fixed. Fig. 7 shows the deformed shape and von Mises stress contour as they resulted from the analysis of Model B for the dead loads only. The maximum stresses that were developed in this case were located at the four columns with a maximum magnitude of 600kPa.

After these first numerical findings were revealed, the stress distribution under the raft slab was studied in order to determine if the considered foundation was able to transfer the superstructure loads to the soil domain in a uniform manner. Fig. 8 shows the von Mises stress distribution that was developed on the soil domain due to the dead loads where it can be seen that the stress field under the shear walls is significantly increased in comparison to the rest of the soil-raft slab interface areas (Model D). Three sections were made in the soil domain to further investigate the stress distribution within the soil (Fig. 9). It can be seen from Fig. 9 that the stress magnitudes increase under the shear walls and the deformations increase were larger in comparison to the areas under the columns. This mechanical behavior is attributed to the fact that the shear walls attract more loads from the slabs and beams connected to them, thus transfer them to the raft slab through their long section (four red lines that appear in Fig. 8). Furthermore, given that the soil is modeled through the use of solid elements, the raft slab is relatively free to deform according to the superstructure loads distribution, which is controlled by the shear walls' and columns' geometry and locations. Even though the raft slab is 70cm thick, the uneven loads applied on the foundation generates uneven stress development at the soil's surface. The maximum von Mises stress that was found from the analysis of the dead loads was 300 kPa, which represents a 33% of the ultimate soil stress.

As it was mentioned above, the 3D detailed approach which is incorporated in the HYMOD method, foresees the modeling of the reinforcement through the use of embedded rebar elements within the hexahedral concrete elements. Fig. 10 shows the deformed shape of the embedded rebar mesh due to the applied dead load on Model D. The embedded rebar mesh deformed shape was similar to that of the concrete mesh given that full bond was assumed. Finally, from this numerical analysis it was also found that the concrete did not develop any cracks when the dead load was applied.

After the completion of the numerical analyses for the dead loads, the seismic load along the negative y axis was applied and a push over analysis was performed for all three models A, B and C. The seismic load distribution was performed according to the Orakdogen *et al*. (2008), while a total of 2350 kN horizontal load was applied incrementally. The horizontal load was distributed at the three beam-column joints located at the back of the structure (Fig. 11) according to the mass distribution of the slab at each floor in order to achieve an objective load distribution. Given the size of the mesh of Model C, the seismic load was applied through the use of 7 load increments in an attempt to decrease the required computational time. The loading strategy foresaw the application of the dead loads and the first horizontal load increment at the first Newton Raphson load step whereas the rest of the seismic load was incrementally applied through the remaining load steps. For the case of Model A, the load was divided into 20 load increments given that the NBCFB element is not as computationally demanding as the 3D detailed model. Table 1 shows the mesh details and the computational time required for each model to be solved (push over analyses). As it can be seen, Model A manages to finish the push over analysis in a minimal computational time (18 seconds). Model B required 4 hours to complete the push over analysis while Model C which was the most computationally demanding required a total of 58 hours.

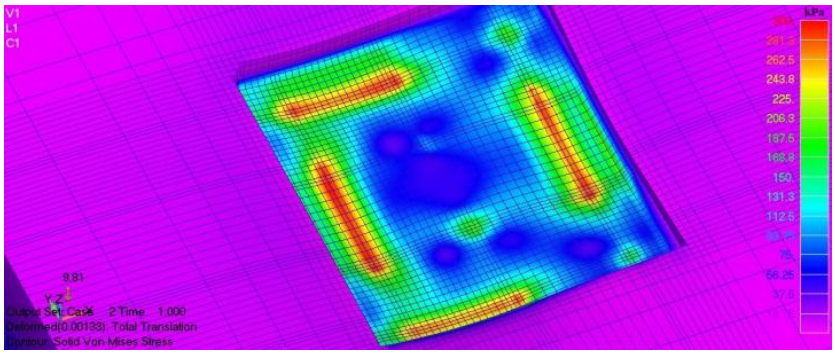

Figure 7 Deformed shape and von Mises stress contour due to the dead loads –Model D – soil domain.

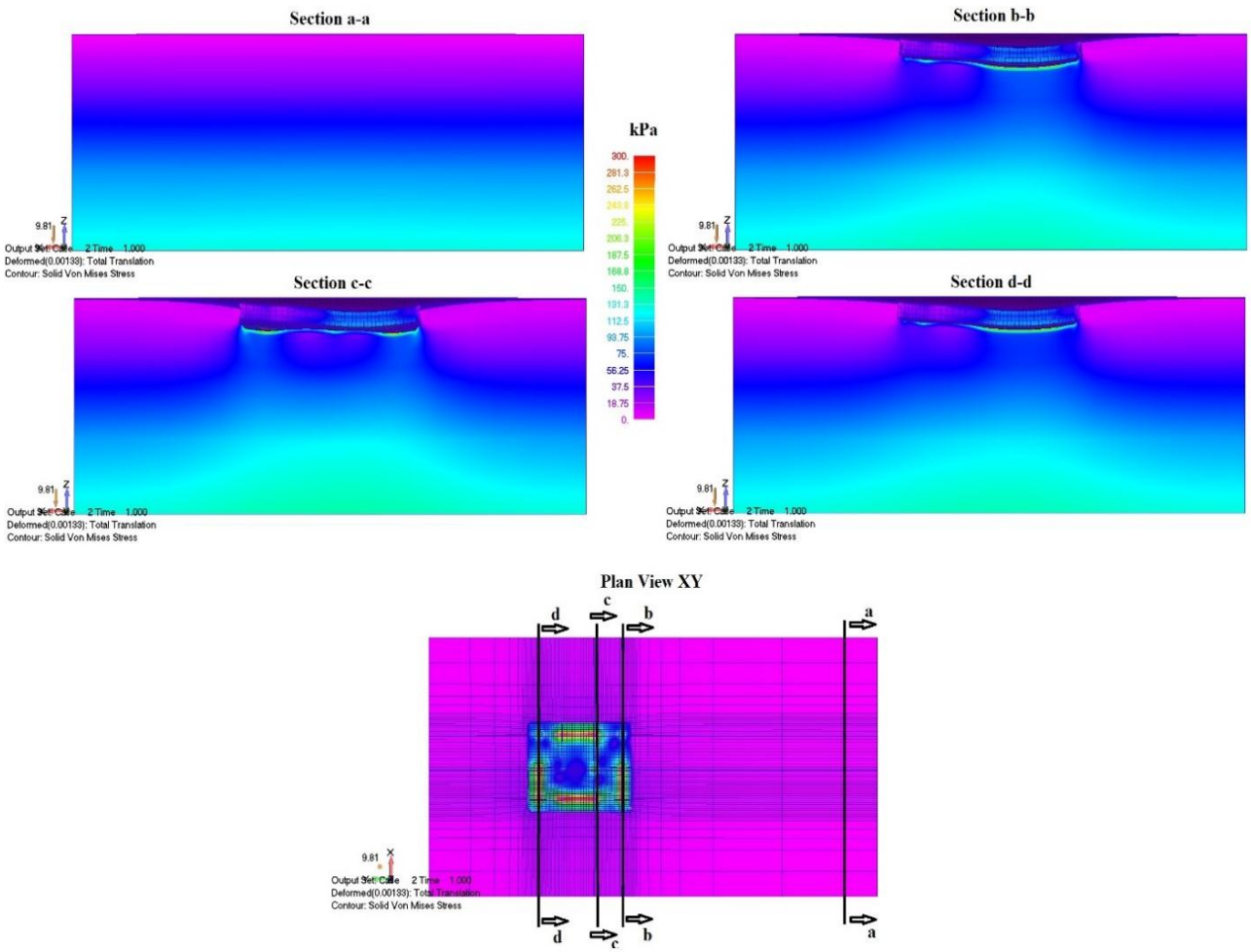

Figure 8 Von Mises stress contours due to the dead loads –Model D – soil domain sections

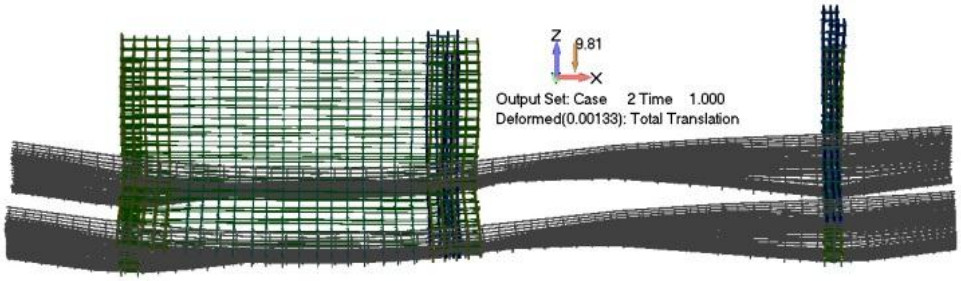

Figure 9 Deformed shape of the embedded rebar mesh of the Model D due to the dead loads

Table 1 Mesh details and computational times required for the push over analysis

Model	Beam Elem.	Rebar Elem.	Concrete Hexa Elem.	Soil Hexa Elem.	Total Elem.	Comp. Time
A	709	-	-	-	709	18 sec
B	685	27,608	8,199	-	36,492	4 hrs
C	685	27,608	8,199	32,493	68,985	58 hrs
Hardware used for the analysis: CPU 3.4 GHz, RAM 16 GB						

Fig. 11 shows the deformed shape of Model A as it resulted from the nonlinear analysis and Fig. 12 shows the deformed shape and the von Mises strain contour prior to failure as it resulted from the analysis of Model B. As it can be depicted from the strain contours, the main strain concentrations are located at the two shear walls parallel to the seismic load. It was also found that the structural system failure was initiated due to the rupture of the longitudinal reinforcement of the beams located at the ground floor. In addition to that the raft slab remained once more undeformed due to the fixed support assumption thus the deformation was mainly observed at the superstructure. In Fig. 13 the crack pattern prior to failure can be seen, where the shear walls that are parallel to the seismic load are the structural members that sustain most of the damages (cracks). It must be noted at this point that a full 3D detailed model needs to be developed in order to investigate the exact mechanical behavior and crack propagation history of the entire frame, while investigate if the modeling of the slabs through the use of rigid beam elements affects significantly the overall push over results.

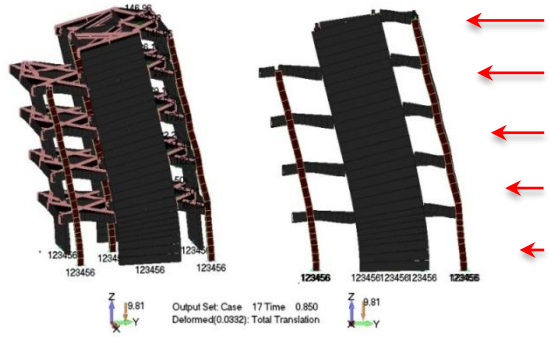

Figure 10 Deformed shape prior to failure – Model A (push over analysis)

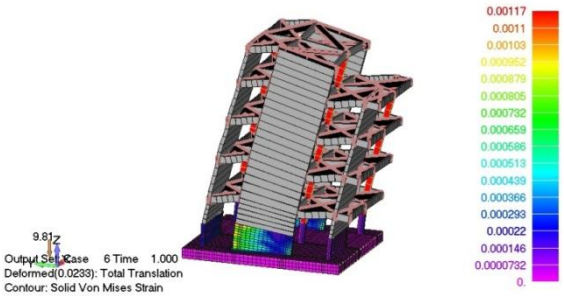

Figure 11 Deformed shape and von Mises strains prior to failure – Model B (push over analysis)

Another interesting finding that resulted from the push over analysis of Model B was the displacement of the frame that was developed along the x axis due to the rotational type of deformation that can be depicted in Fig. 14 (a). This is attributed to the positioning of the shear walls that are perpendicular to the applied seismic load that generate an eccentricity along the x axis. The rotational deformation of the shear wall located at the back of the structure can be seen in Fig. 14 (b). This type of behavior (shear wall deformation due to torsion) was not captured by Model A given that the frame was solely discretized with NBCFB (beam) elements.

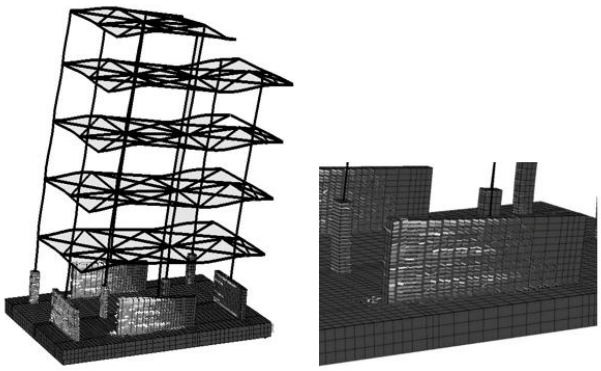

Figure 12 Deformed shape and crack pattern prior to failure for the case of Model B (push over analysis)

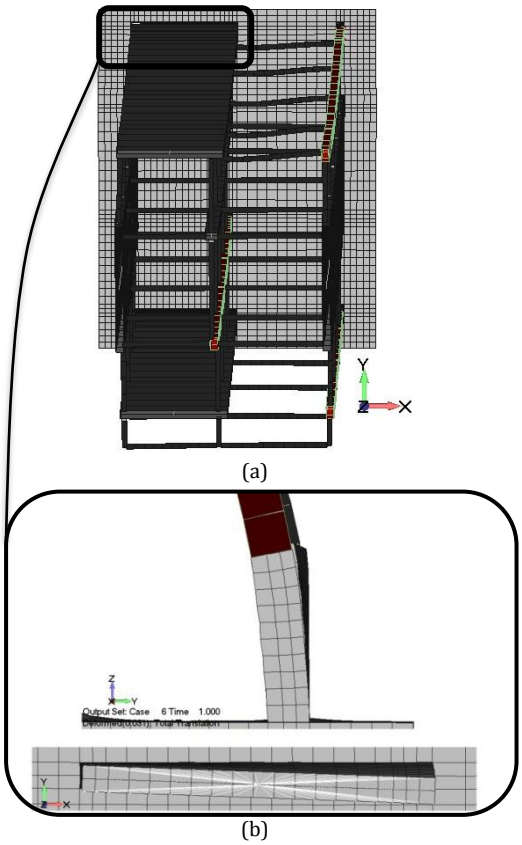

Figure 13 (a) Top view of the deformed shape of the frame and (b) side view and top view of the shear wall prior to failure for the case of Model B (push over analysis)

The crack openings due to the seismic loads initiated at the shear walls that were parallel to the y-axis, (seismic load direction) in the form of horizontal cracks at the base of the shear walls within the tensile region (due to the bending moment). Fig. 15 shows the inside view of the crack pattern development of these shear walls and the raft slab prior to failure. It can be easily observed that the tensile cracks (horizontal cracks) are transferred to the raft slab under the tensile region of the shear walls. This phenomenon is attributed to the significant tensile stresses that are developed at the shear wall's longitudinal embedded rebars, which transfer the stresses to the concrete domain. The tensile stresses pull the concrete domain thus cracking occurs within the raft slab. According to the numerical results derived from Model B, this is the only region of the raft slab that will develop cracks due to this seismic load. Finally the maximum horizontal displacement of Model B was 23.3mm for a total of 2015 kN horizontal load (failure occurred at load step 7).

The third finite element mesh (Model C) was also used to perform a push over analysis in order to determine the structural seismic capacity along the y axis and investigate the SSI effects. Fig. 16 illustrates the deformed shape and the von Mises strain contours prior to failure in the raft slab and half of the ground floor that was model through the use of solid finite elements. As it can be seen, the strain distribution is similar to the one derived from Model B, with differences found mainly within the raft slab.

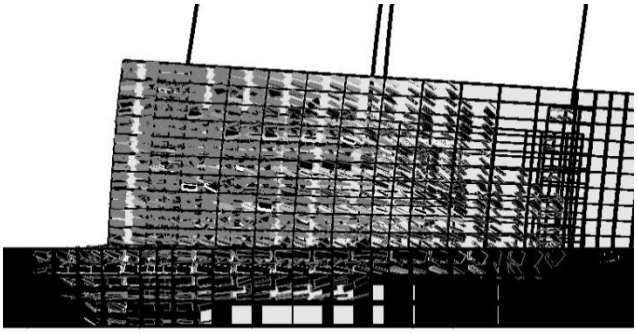

Figure 14 Crack pattern inside the shear walls and raft slab prior to failure – Model B (push over analysis)

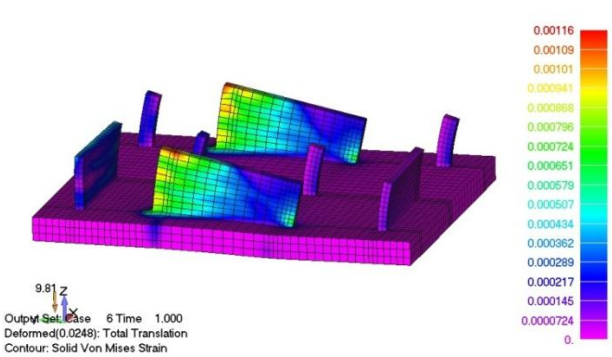

Figure 15 Deformed shape and von Mises strain contour prior to failure – Model C (push over analysis)

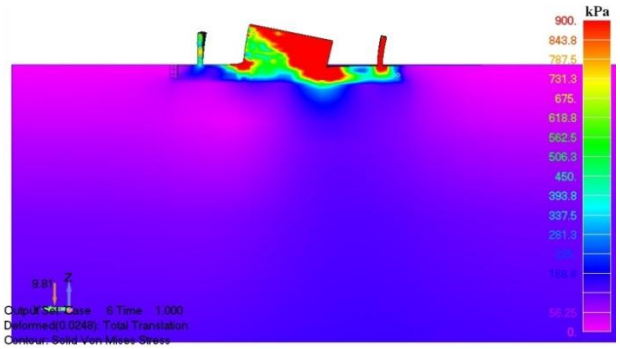

Figure 16 Deformed shape and von Mises stress contour - prior to failure – Model C (push over analysis)

In addition to the above, when a section was performed (see Fig. 17), it was revealed that the raft slab undertook a certain level of deformation (Fig. 19) that was not captured from the numerical results derived from Model B (Fig. 12). Even though the raft slab minimizes the SSI effect (it behaves like a stiff base for the shear walls and columns), it develops a bending type of deformation that eventually leads to a stress field redistribution. As it derives from this research work, the crack pattern that resulted from the analysis of Model C was different from the crack pattern derived from Model B, especially within the raft slab of the building.

Fig. 18 illustrates the von Mises stress contour on the interface of the foundation with the soil domain as it resulted from the analysis of Model C, for the seismic loads. It is easy to observe that the main stress development takes place under the compressive region of the two shear walls that are parallel to the applied seismic load (parallel to the y-axis). According to this analysis the maximum developed von Mises stress at the soil domain interface with the RC raft slab, was close but not larger than 900 kPa thus this indicates that the soil did not reach its maximum strength and behaved in an elastic manner throughout the nonlinear analysis.

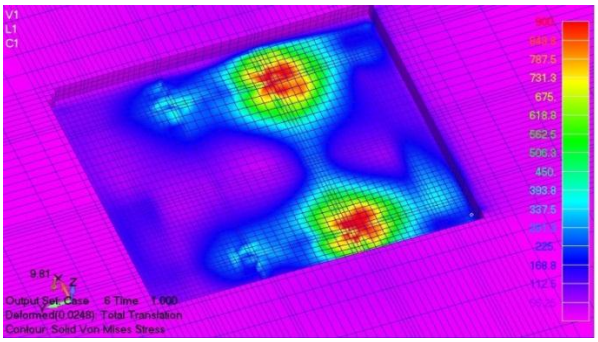

Figure 17 Deformed shape and von Mises stress contour of the soil domain interface – Model C (push over analysis)

Regarding the deformation shape of the raft slab, Fig. 19 shows clearly that the foundation bends due to the

excessive compressive load that is transferred from the two shear walls (due to the developed bending moments), while the displacement contours of the raft slab's base has negative values (settlement), indicating that the raft slab did not develop any uplift.

Fig. 20 shows the crack pattern that was developed prior to failure for the case of Model C where it can be seen that the shear walls are the structural members that sustain most of the damage at the ground floor. After visually switching off the hexahedral elements in order to observe the crack openings inside the raft slab (see Fig. 21), it was found that additional cracks occurred under the compressive zone of the two shear walls that are parallel to the seismic load. These cracks occurred at the area where the raft slab bends, while this finding is attributed to the SSI effect and the ability of the foundation to deform. Finally, Fig. 22 shows the P-δ curves of the three models as they resulted from the push over analyses. As it can be observed, Model A exhibits a stiffer behavior due to its inability to capture the shear deformation that occurs in the two main shear walls while it fails at a higher seismic load in comparison to models B and C. Model B derives a more flexible behavior due to its ability to account for the shear deformation but it exhibits a stiffer behavior in relation to Model C which accounts for the SSI phenomenon. It is also evident that the SSI effect is not significant in this problem at hand due to the large stiffness of the foundation and the underlying soil. To derive a more comprehensive conclusion on the effect of SSI on the response of the studied building several soil types from different soil classes should be studied.

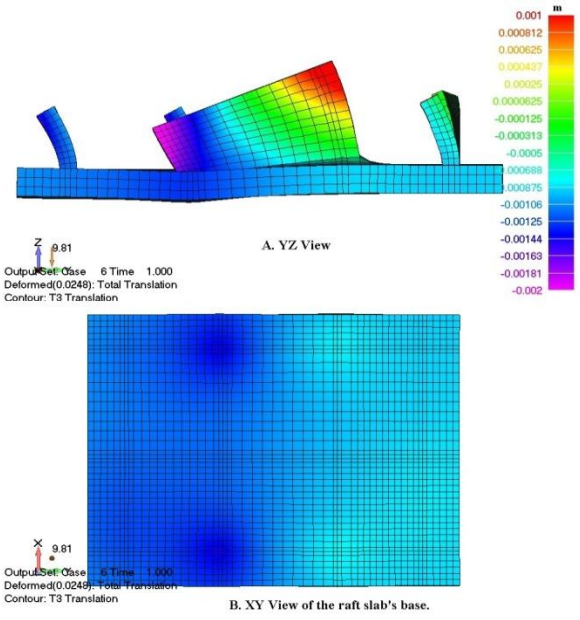

Figure 18 Deformed shape and z-axis translation contour prior to failure – Model C (push over analysis).

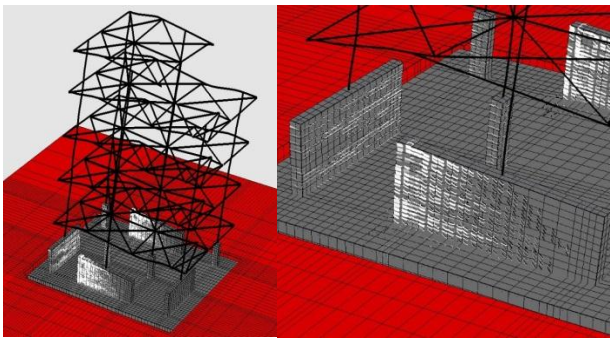

Figure 19 Crack pattern and deformed shape prior to failure – Model C (push over analysis)

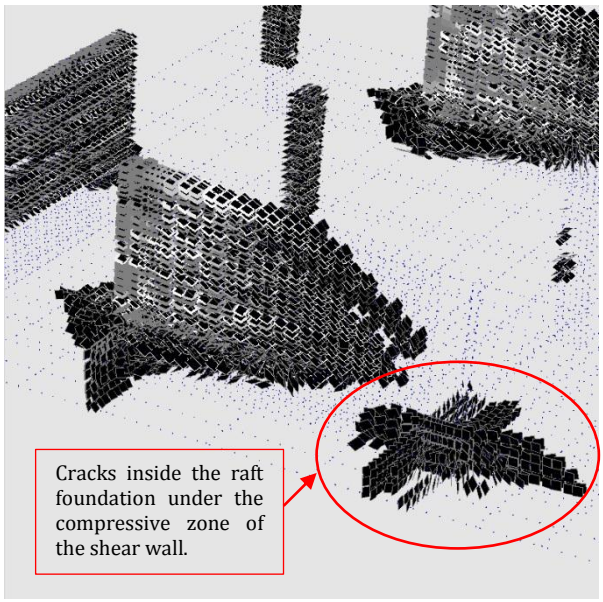

Figure 20 Crack pattern inside the raft slab and shear walls prior to failure – Model C (push over analysis)

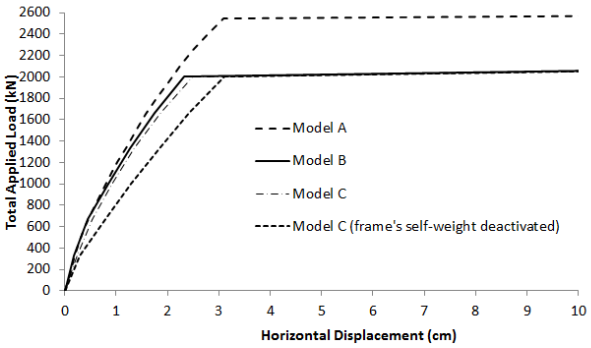

Figure 21 P-δ curves

Conclusions and Future Work

A numerical investigation was performed to study the effect of SSI on the response of a retrofitted 5-storey building through the use of HYMOD numerical models. Three main models were developed and numerically analyzed for linear and nonlinear loads.

From this research work several findings resulted, while future work is required to derive additional conclusions on the SSI local and overall effects. The main findings from this numerical investigation are summarized below:

1) Full scale 3D modeling of RC structures with supporting foundation and soil for studying the SSI effect is feasible through the use of the HYMOD method.
2) A HYMOD model was developed for a 5-storey reinforced concrete retrofitted building. The numerical model was used to perform push over analysis and the derived results were compared with those of a more simplified beam-column finite element model. It was found that the shear effect plays an important role when modeling shear walls. Furthermore, the beams of the structure were found to be responsible for leading the structure to failure given that their longitudinal reinforcement failed first (a full 3D-detailed model is required to be developed so as to further investigate the mechanical response of the studied building and especially the contribution of the slab's stiffness to the overall mechanical response of the building).
3) When supporting our building on a stiff raft slab the SSI effect is minimized. Additional soil material properties (softer soil) have to be considered in future analyses so as to derive an objective conclusion for the overall SSI effect.
4) When the SSI is accounted for (Model C), the overall mechanical behavior of the building becomes more flexible. In addition to that the stress distribution and the deformed shape of the raft slab differed from that of the fixed base Model B that did not model the soil. For the case where the seismic loads are applied on Model C, the raft slab develops deformation which leads to additional crack development.
5) For the case of Model C, it was found that the stress distribution underneath the raft slab was not uniform (for both dead and seismic loads) thus it was controlled by the vertical structural members (columns and shear walls) connected to it. The soil domain developed different stress contours at the interface area with the raft slab, thus its stress distribution varied accordingly. In addition to that it was found that the soil did not exceed its ultimate strength thus it was within the elastic region for both dead and seismic loading cases. This is mainly attributed to the stiff behavior of the raft slab that manages to maintain low stress levels on the interface area with the soil domain.
6) The structure was found to be irregular thus develop a rotational type of deformation due to the seismic loads applied along the y-axis. For this reason, additional torsion was developed in structural members within the framing system of the structure.
7) The model that accounted for the SSI phenomenon (Model C) revealed that the raft slab did not develop any uplifts due to the seismic load.
8) Different foundation types need to be considered in future work so as to further investigate the mechanical response of the SSI problem under 3D considerations.
9) The SSI effect that was incorporated in Model C by discretizing the soil domain with hexahedral elements was found to be computationally demanding. For this reason, ReConAn FEA needs to be integrated with a parallel solver (this is a future programing task).

Acknowledgements

The authors would like to thank Dr. Engin Orakdogen for his help in providing data related the 5-storey RC building.

References

Baragani, R. and Dyavanal, S.S. (2014), Performance based seismic evaluation of G+6 RC buildings considering soil structure interaction, *International Journal of Engineering Trends and Technology*, 14(3), pp. 119-127.

Filippou, F.C., Popov, E.P. and Bertero, V.V. (1983), Effects on Bond Deterioration on Hysteretic Behavior of Reinforced Concrete Joints, EERC Report 83-19, Earthquake Engineering, Research Center, Berkeley.

Gonzalez-Vidosa F., Kotsovos M.D. and Pavlovic M.N. (1991), A three-dimensional nonlinear finite-element model for structural concrete. Part 1: main features and objectivity study; and Part 2: generality study, Proceedings of the Institution of Civil Engineers, Part 2, Research and Theory, Vol. 91, pp. 517-544.

Halkude, S.A., Kalyanshetti, M.G. and Kadlag, V. A. (2015), Pushover analysis of R.C. frames considering soil structure interaction, *International Journal of Current Engineering and Technology*, 5(1), pp. 167-171.

Ismail, A. (2014), Effect of soil flexibility on seismic performance of 3-D frames, *IOSR Journal of Mechanical and Civil Engineering*, 11(4), pp. 135-143.

Kent, D.C. and Park, R. (1971), Flexural Members with Confined Concrete, Journal of the Structural Division, ASCE, 97(ST7).

Khoshnoudian, F. and Behmanesh, I. (2010), Evaluation of FEMA-440 for including soil-structure interaction, *Earthquake Engineering and Engineering Vibration*, 9(3), pp. 397-408.

Kotsovos M.D. (1983), Effect of Testing Techniques on the Post-Ultimate Behavior of Concrete in Compression, Materials & Structures, RILEM, Vol. 16(91), pp. 3-12.

Kotsovos M.D. and Pavlovic M.N. (1995), Structural concrete. Finite Element Analysis for Limit State Design, Thomas Telford, London.

Liu, L., Gou, W., Xie, Q, Bi, L. Li, Y. and Wu, Y. (2012), Analysis of elasto-plastic soil structure interaction system using pushover method, *Proceedings of the 15th World Conference on Earthquake Engineering*, Lisboa, Portugal, September 24-28, 2012, pp 6.

Liu, L., Xia, K. and Cao, X. (2008), The research of applied pushover method in the earthquake resistance analysis of

soil-structure interaction system, *Proceedings of the 14th World Conference on Earthquake Engineering,* Beijing, China, October 12-17, 2008, pp 7.

Makhmalbaf, M.O., GhanooniBagha, M. Tutunchian, M.A. and Samani, M.Z. (2011), Pushover analysis of short structures, International Scholarly and Scientific Research and Innovation, World Academy of Science, Engineering and Technology, 5(3), pp. 242-246.

Markou G. (2011), Detailed Three-Dimensional Nonlinear Hybrid Simulation for the Analysis of Large-Scale Reinforced Concrete Structures, Ph.D. Thesis, National Technical University of Athens.

Markou G. and Papadrakakis M. (2013), Accurate and Computationally Efficient 3D Finite Element Modeling of RC Structures, Computers & Concrete, 12(4), pp. 443-498.

Markou G. and Papadrakakis M. (2014), "A Simplified and Efficient Hybrid Finite Element Model (HYMOD) for Non-Linear 3D Simulation of RC Structures", Engineering Computations, In Press, Accepted for Publication Oct. 2014.

Markou, G. (2010), ReConAn v1.00. Finite Element Analysis Software Manual, Institute of Structural Analysis and Seismic Research, Technical University of Athens, Greece.

Mathew, J.M., Cinitha, A., Iyer, N.R. and Sakaria, E. (2014), Seismic response of RC building by considering soil structure interaction, *International Journal of Structural and Civil Engineering Research*, 3(1), pp. 160-175.

Menegotto M. and Pinto P.E. (1973), Method of Analysis for Cyclically Loaded Reinforced Concrete Plane Frames Including Changes in Geometry and Non-Elastic Behavior of Elements under Combined Normal Force and Bending, Proceedings, IABSE Symposium on Resistance and Ultimate Deformability of Structures Acted on by Well Defined Repeated Loads, Lisbon, pp. 15-22.

Orakdogen, E., Girgin, K., Boduroglu, M.H., Buyuksisli, B. and Gokce, T. (2008), Performance evaluation of a strengthened building considering the soil structure interaction, *Journal of Earthquake Engineering*, 12(S2), pp. 222-233.

Panagiotidou, A., Gazetas, G., and Gerolymos, N. (2012), Pushover and seismic response of foundations on stiff clay: Analysis with P-Delta effects, *Earthquake Spectra*, 28(4), pp. 1589-1618.

Rashid Y.M. (1968), Ultimate strength analysis of prestressed concrete vessels, Nucl Eng and Des, Vol. 7, pp. 334-344.

Van Mier J.G.M. (1986), Multiaxial strain-softening of concrete. Materials & Structures, RILEM, Vol. 19(111), pp. 179-200.

Van Mier J.G.M., Shah S.P., Arnaud M., Balayssac J.P., Bassoul A., Choi S., Dasenbrock D., Ferrara G., French C., Gobbi M.E., Karihaloo B.L., Konig G., Kotsovos M.D., Labnz J., Lange-Kornbak D., Markeset G., Pavlovic M.N., Simsch G., Thienel K.C., Turatsinze A., Ulmer M., van Vliet M.R.A., and Zissopoulos D. (1997), (TC 148-SSC: Test methods for the strain-softening of concrete), Strain-softening of concrete in uniaxial compression, Materials & Structures RILEM, Vol. 30(198), pp. 195-209.Zhao, L. and Wang J.H., (2008),

Vertical bearing capacity for ring footings, *Computers and Geotechnics*, 35, pp. 292-304.

Appendix A: 3D Concrete Material Model with Smeared Cracking

The experimental data on concrete behavior used for the development of constitutive laws are obtained from tests on specimens such as cylinders, prisms and cubes. Such specimens are subjected to various load combinations, usually applied through rigid steel plates (compressive test or triaxial test). The obtained results are expressed in the form of stress-strain curves, which consist of a strain hardening branch followed by a strain softening one. After extensive experimental work (Kotsovos, 1983, van Mier, 1986 and van Mier *et al*., 1997), it was found that only strain hardening may describe material behavior under a definable state of stress. It was concluded that the strain softening branch basically reflects the interaction between specimens and loading platens (Fig. A1), with the development of uncontrolled frictional stresses on the faces between the specimen and the loading device.

The generalized stress-strain relationships, corresponding to the ascending branch of concrete materials, can be expressed by decomposing each state of stress into a hydrostatic (σ_0) and a deviatoric component (τ_0) which represent the normal and shear octahedral stresses. The hydrostatic and deviatoric stresses derive from the corresponding hydrostatic and deviatoric strains (ε_0, γ_0) from the following relationships:

$$\varepsilon_0 = \varepsilon_{0h} + \varepsilon_{0d} = \frac{\sigma_0 + \sigma_{id}}{3K_S}, \qquad \gamma_0 = \frac{\tau_0}{2G_S} \tag{a1}$$

where σ_{id} (σ_0,τ_0,f_c) is an equivalent internal hydrostatic stress that accounts for the coupling between τ_0 and ε_{0d}, K_S (σ_0,τ_0) and G_S (σ_0,τ_0) are secant bulk and shear moduli, respectively, obtained by ignoring the coupling stress σ_{id}. The expressions for σ_{id}, K_S and G_S, can be found in Kotsovos and Pavlovic, (1995).

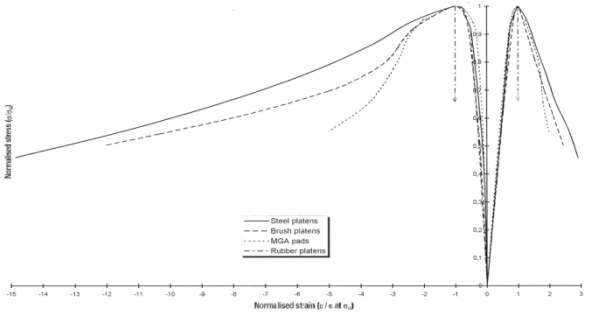

Figure A1 Stress-strain curves for different types of boundary conditions of the experimental setup (van Mier *et al*., 1997).

Since σ_{id} is a pure hydrostatic correction, the expressions in Eqs. a1 are equivalent to the following relations which are written in the global coordinate system:

$$\varepsilon_{ij} = \frac{\sigma_{ij} + \sigma_{id}\delta_{ij}}{2G_S} - \frac{3\nu_S}{E_S}\left(\sigma_0 + \sigma_{id}\right)\delta_{ij} \tag{a2}$$

where $E_S(\sigma_0,\tau_0,f_c)$ and $\nu_S(\sigma_0,\tau_0,f_c)$ are secant Young's modulus and Poisson's ratio derived from K_S and G_S, using the standard expressions of linear elasticity

$$E_S = \frac{9K_S G_S}{3K_S + G_S}, \qquad \nu_S = \frac{3K_S - 2G_S}{6K_S + 2G_S} \tag{a3}$$

The nonlinear deformation component of concrete corresponding to τ_0 is considerably larger than that for σ_0 and if $max\ \tau_0$ corresponds to the maximum deviatoric stress at each point on the stress-strain curve, then the elastic unloading/reloading occurs whenever the deviatoric stress τ_0 becomes less than $max\ \tau_0$.

The octahedral stresses are used to describe the failure of the concrete, which may be represented in the three-dimensional principal stress space by an open and convex failure surface. The projection of the failure surface on the deviatoric plane, which is normal to σ_0, results in a curve that represents the geometric locus of the ultimate deviatoric stress τ_{0u} (Kotsovos and Pavlovic, 1995). This ultimate stress may be calculated from σ_0 and θ, where θ is the rotational angle that the deviatoric stress vector forms with one of the projected stress principal axes on the deviatoric plane:

$$\tau_{0u} = \frac{2\tau_{0c}\left(\tau_{0c}^2 - \tau_{0e}^2\right)cos\theta + \tau_{0c}\left(2\tau_{0e} - \tau_{0c}\right)\sqrt{\left[4\left(\tau_{0c}^2 - \tau_{0e}^2\right)cos^2\theta + 5\tau_{0e}^2 - 4\tau_{0c}\tau_{0e}\right]}}{4\left(\tau_{0c}^2 - \tau_{0e}^2\right)cos^2\theta + \left(\tau_{0c} - 2\tau_{0e}\right)^2} \tag{a4}$$

This expression describes a smooth convex curve with tangents perpendicular to the directions of τ_{0e} and τ_{0c} at $\theta = 0^o$ and $\theta = 60^o$, respectively (Fig. A2). Therefore, a full description of the strength surface can be established when the variants of σ_0, τ_{0e}, and τ_{0c} are determined. A mathematical description of the two strength envelopes may be obtained as previously, by fitting curves to the experimental data.

The Kotsovos and Pavlovic material model, assumes a nonlinear behavior for the moduli K_S and G_S (Kotsovos and Pavlovic, 1995) for very low values of $\tau_{0u} << max\ \tau$. The updating of the hexahedral stiffness matrices, at the early stages of loading, demands extra computational effort with no measured effect on the structural behavior. Thus, in the Kotsovos and Pavlovic material model formulation, it is necessary to update the material constitutive matrix at each hexahedral Gauss point according to the change of K_S and G_S moduli. Having to solve an ill-posed numerical problem when cracking occurs, the uncracked hexahedral elements induce additional numerical instability, as a result of the unbalanced forces produced due to the update of the material constitutive matrix. This increases the computational cost due to the requirement for a continuous stiffness update.

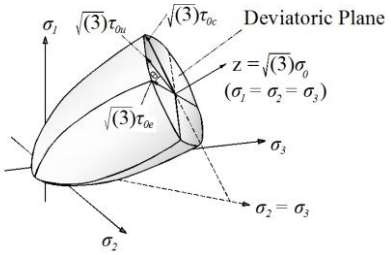

(a)

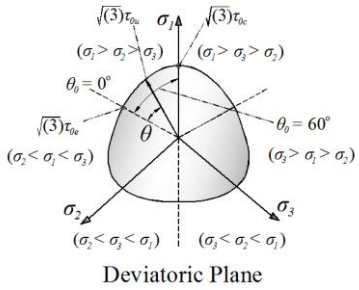

(b)

Figure A2 Schematic representation of the ultimate-strength surface. (a) General view in stress space; (b) Typical cross-section of the strength envelope coinciding with a deviatoric plane. (Markou and Papadrakakis, 2013)

Following a parametric investigation it was concluded that if the ultimate deviatoric stress τ_{0u} at any Gauss point is less than 50% of the corresponding ultimate strength (Eq. a4), then the elastic constitutive matrix $\boldsymbol{C}$ can be retained in the formulation of the stiffness matrix. It is only when the deviatoric stress τ_{0u} exceeds 50% of the corresponding ultimate strength that the nonlinear material law is activated and the constitutive matrix is computed by updating the K_T and G_T moduli. Fig. A3 illustrates the flow chart of the proposed numerical handling of the material model (Markou and Papadrakakis, 2013).

Smeared crack models take into consideration crack openings by modifying the calculation of stiffness matrices and stresses at corresponding integration points. This approach proceeds with the simulation of individual cracks without the need for remeshing, as it is required for the case of the discrete-crack approach where a physical gap in the FE mesh is introduced at the location of the crack.

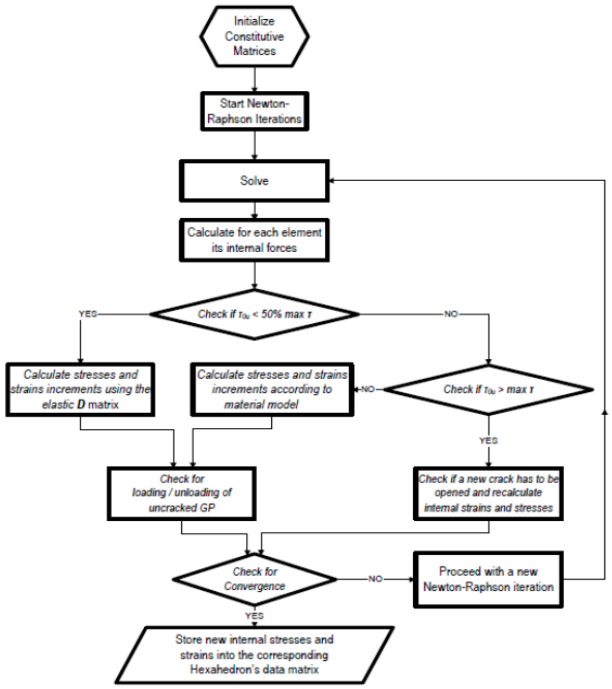

Figure A3 Flow chart of the adopted concrete material model. (Markou and Papadrakakis, 2013)

The smeared crack model implemented in this work is based on the work of Rashid, 1968 as described by Gonzalez-Vidosa *et al.*, 1991. In the framework of an incremental iterative procedure the increments of stresses at each Gauss point are found from the increments of strains through the constitutive matrix $\boldsymbol{C}$.

$$\Delta\boldsymbol{\sigma} = \boldsymbol{C}\cdot\Delta\boldsymbol{\varepsilon} \qquad \text{(a5)}$$

A crack occurs when the ultimate deviatoric stress τ_{0u} at a Gauss point has been exceeded (usually in tension or in combination of tension and compression). Then a plane is formed (crack's plane) which is perpendicular to the direction of the maximum tensile stress that exists before cracking. This tensile stress is set to zero inducing unbalanced forces at the element nodes. The incremental stress-strain relation of Eq. a5 is transformed to the corresponding Cartesian axes (x', y', z') of the crack before properly adjusted to take into consideration zero stress along the perpendicular axis to the plane of crack (*axis* z') and a modified shear rigidity G along the plane of crack:

$$\begin{Bmatrix}\Delta\sigma'_x\\ \Delta\sigma'_y\\ \Delta\sigma'_z\\ \Delta\tau'_{xy}\\ \Delta\tau'_{yz}\\ \Delta\tau'_{zx}\end{Bmatrix} = \begin{bmatrix}2G+\mu & \mu & . & . & . & .\\ \mu & 2G+\mu & . & . & . & .\\ . & . & . & . & . & .\\ . & . & . & G & . & .\\ . & . & . & . & \beta G & .\\ . & . & . & . & . & \beta G\end{bmatrix}\cdot\begin{Bmatrix}\Delta\varepsilon'_x\\ \Delta\varepsilon'_y\\ \Delta\varepsilon'_z\\ \Delta\gamma'_{xy}\\ \Delta\gamma'_{yz}\\ \Delta\gamma'_{zx}\end{Bmatrix} \qquad \text{(a6)}$$

where μ is the Lamé constant. A schematic representation of the planes of cracks and the corresponding axis is depicted in Fig. A4.

Following this crack formulation, if a tensile state of stress is reached in a different direction at a subsequent load level, then a second crack opens with its corresponding plane being perpendicular to the direction of the new maximum principal tensile stress. Hence, in combination with the previous state of stress, non-zero stress can only be developed along the intersection of the two planes (Fig. A4). Consequently, the incremental stress – strain relations along these Cartesian axes (x'', y'', z'') are given by

$$\begin{Bmatrix}\Delta\sigma''_x\\ \Delta\sigma''_y\\ \Delta\sigma''_z\\ \Delta\tau''_{xy}\\ \Delta\tau''_{yz}\\ \Delta\tau''_{zx}\end{Bmatrix} = \begin{bmatrix}. & . & . & . & . & .\\ . & 2G+\mu & . & . & . & .\\ . & . & . & . & . & .\\ . & . & . & \beta G & . & .\\ . & . & . & . & \beta G & .\\ . & . & . & . & . & \beta G\end{bmatrix}\cdot\begin{Bmatrix}\Delta\varepsilon''_x\\ \Delta\varepsilon''_y\\ \Delta\varepsilon''_z\\ \Delta\gamma''_{xy}\\ \Delta\gamma''_{yz}\\ \Delta\gamma''_{zx}\end{Bmatrix} \qquad \text{(a7)}$$

In the event that a third tensile stress occurs in a different direction at the same Gauss point, then a zero stiffness contribution is assumed for this specific Gauss point.

Parameter β plays an important role in most cases, when using the smeared crack approach, as a result of its contribution to the stability of the nonlinear iterative procedure when cracks open. If this parameter is set to zero with the creation of a crack, then zero diagonal terms may appear in the global stiffness matrix, particularly when the RC structure is sparsely reinforced. The physical meaning of this parameter is related to the remaining stiffness due to aggregate interlocking along the cracks surface. An acceptable value for this variable is $\beta = 0.1$ which was extracted from experimental data. This implies that 10% of the initial shear strength is remaining after the opening of the crack as a result of the aggregate interlocking along the crack's plane (Markou and Papadrakakis, 2013).

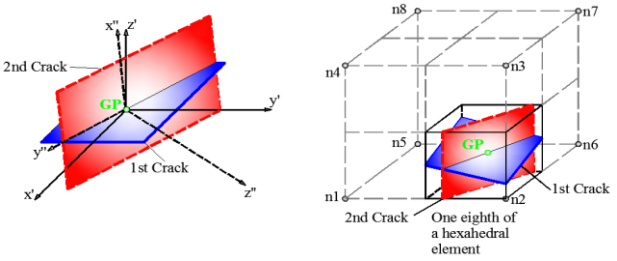

Figure A4 Local axes for the case of two cracks at a specific Gauss point

Appendix B: Menegotto & Pinto Material Model for Steel

Reinforcement steel bars are modeled in the case of the NBCFB fiber element with the Menegotto and Pinto, (1973) steel material model (Fig. B1) and the Filippou et. al., (1983) isotropic hardening which is assigned to the fibers of the NBCFB element. Despite the numerical simplicity of this model it provides the required accuracy and robustness in modeling the numerical response of steel reinforcement which mainly exhibits uniaxial behavior.

In the HYMOD approach shear dominated structural members are modeled with 8-noded isoparametric hexahedral elements for the concrete and the 2-noded rod or the NBCFB fiber beam elements for modeling the embedded reinforcement located inside the concrete domain, as implemented by Markou and Papadrakakis, (2013).

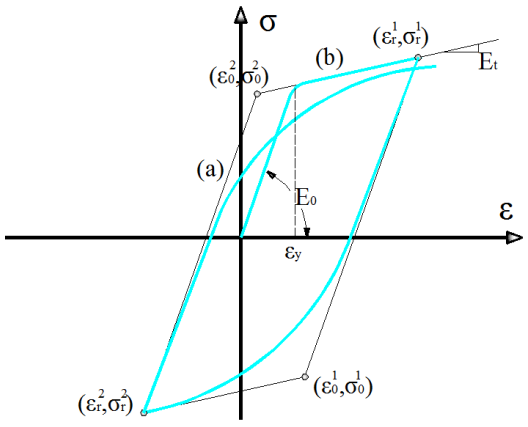

Figure B1 Menegotto – Pinto steel model

Appendix C: Kent & Park Material Model for Concrete

The HYMOD approach considers two different types of FE models that their formulation is based on one- and three-dimensional domains, two different material models are adopted. For the case of the NBCFB fiber element the concrete is modeled through the use of the modified Kent-Park, 1971 concrete model. This model (Fig. C1) offers simplicity and accuracy and is considered to be arithmetically efficient and convenient for 1D concrete material modeling. For the case of the NBCFB fiber element, each concrete fiber is assigned to a maximum tensile stress which is connected to the cylindrical compressive strength of the material characteristics of concrete.

In our numerical implementation the tensile strength of concrete was set to 5% of the corresponding cylindrical uniaxial compressive strength, while cracking along the section of the structural beam is accounted for.

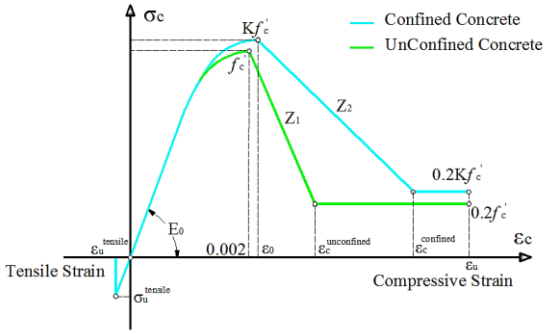

Figure C1 Kent – Park concrete model with tensile strength for monotonic loading.